

Article

Crystal Chemistry and Structural Variations for Zircon Samples from Various Localities

M. Mashrur Zaman and Sytle M. Antao * 

Department of Geoscience, University of Calgary, Calgary, AB T2N 1N4, Canada; mmzaman@ucalgary.ca

* Correspondence: antao@ucalgary.ca

Received: 23 September 2020; Accepted: 21 October 2020; Published: 25 October 2020



Abstract: This study investigates the variations of structural parameters and chemistry of a partially metamict and seven detrital zircon samples from different localities using single-crystal X-ray diffraction, synchrotron high-resolution powder X-ray diffraction, and electron-probe micro-analysis techniques. The unit-cell parameters for the eight zircon samples vary linearly with increasing unit-cell volume, V . A zircon sample from the Canadian Arctic Islands has the smallest unit-cell parameters, bond distances, ideal stoichiometric composition, unaffected by α -radiation damage, and is chemically pure. A zircon sample from Jemaa, Nigeria has the largest unit-cell parameters because of the effect of α -radiation doses received over a long time (2384 Ma). All the samples show good correlations between Zr and Si *apfu* (atom per formula unit) versus unit-cell volume, V . The α -radiation doses in the samples are lower than $\sim 3.5 \times 10^{15}$ α -decay events/mg. Substitutions of other cations at the Zr and Si sites control the variations of the structural parameters. Relatively large unit-cell parameters and bond distances occur because the Zr site accommodates other cations that have larger ionic radii than the Zr atom. Geological age increases the radiation doses in zircon and it is related to V .

Keywords: zircon; crystal structure; chemical analysis; crystal chemistry; α -radiation damage

1. Introduction

Variations of structural parameters in zircon in relation to the contents of Zr, Si, and α -radiation damage are important because they control the stability of zircon. The crystal structure of zircon was first determined by Vegard [1] and confirmed by others [2–4]. The crystal structure of gem quality and synthetic zircon samples were studied under ambient conditions and elevated pressure and temperature conditions [5–9].

The ideal chemical formula for zircon is ZrSiO_4 (formula unit, $Z = 4$) and the space group is $I4_1/amd$. Zircon is an orthosilicate and its structure consists of isolated SiO_4 tetrahedra and ZrO_8 dodecahedra (Figure 1). The SiO_4 and ZrO_8 polyhedra share edges to form chains parallel to the c axis (Figure 1a). The SiO_4 tetrahedron is a tetragonal disphenoid (symmetry $2m$) elongated parallel to [1] because of repulsion between Zr^{4+} – Si^{4+} cations, whose polyhedra share a common edge [9]. The Zr atom is coordinated to eight O atoms and forms a dodecahedron with symmetry $2m$. According to Nyman et al. [10], the ZrO_8 dodecahedron in zircon can be described as two interpenetrating ZrO_4 tetrahedra in which one is elongated along [1] and the other is compressed along [100] and [10].

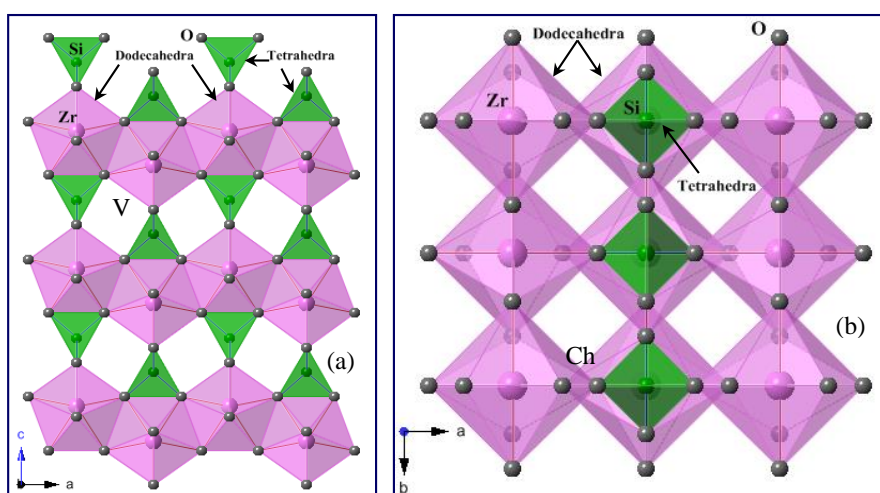


Figure 1. Polyhedral representation of the zircon structure, which consists of isolated SiO_4 tetrahedra and ZrO_8 dodecahedra that share their (a) edges with each other to form a chain parallel to c axis, and (b) corners with other ZrO_8 dodecahedra along the a and b axes. There are small voids [V in (a)] and open channels [Ch in (b)] between SiO_4 and ZrO_8 polyhedra.

Zircon is one of the most incompressible silicate minerals and its unit-cell parameters decrease with increasing pressure [6]. The unit-cell parameters of metamict zircon increase with increasing temperature [8]. The increase in a and c unit-cell parameters arises from expansion of the ZrO_8 polyhedra, but the overall shape of the SiO_4 tetrahedra remains essentially undistorted in partially metamict zircon [11]. In synthetic zircon, the Zr^{4+} cation is strongly bonded and its vibrational behavior is not strongly anisotropic [7]. The limits of rare earth elements (REE) and P atom incorporations in the Zr and Si sites in zircon structure depend on not only the ionic radii of REE and P atom, but also the structural strain at the Zr and Si sites [5]. Small voids and open channels in between SiO_4 and ZrO_8 polyhedra are considered as potential interstitial sites for impurity atoms (Figure 1). Such sites can accommodate interstitial atoms without excessive structural strain [12]. The role of these interstitial sites is unknown.

This study examines the structural variations and α -radiation damage in zircon from different localities. Several structural trends are observed and explained on the basis of crystal-chemical principles. This study shows some trends among structural (unit-cell parameters and bond distances), chemical composition (Zr, Si, Hf, and TE), and α -radiation doses.

2. Experimental Methods

2.1. Sample Description

Seven detrital and one partially radiation damaged metamict zircon samples were used in this study. Samples 1 to 4 are from Cox's Bazar (CB), Bangladesh, samples 5 to 7 are from the Canadian Arctic Island, and sample 8 is from Jemaa, Nigeria (JN).

Zircon fraction was separated from a raw beach placer sand sample with gravity, conductivity, and magnetic separators at Beach Sand Minerals Exploitation Centre, Bangladesh. The zircon fractionation technique for the beach placer sands was described by Zaman et al. [13]. Using a stereomicroscope, (1) colorless, (2) pink, (3) gray, and (4) red zircon crystals were selected from the detrital zircon fraction. Three more detrital zircon samples were separated from samples collected from three sedimentary formations: (5) Beverly Inlet Formation (BIF; GSC #C198959), (6) Hecla Bay Formation (HBF; GSC #C246257), and (7) Parry Islands Formation (PIF; GSC #C245984) of the Franklinian Basin, Canadian Arctic Islands, Canada. The separation technique for samples 5 to 7 is given by Anfinson et al. [14]. All zircon samples were examined with a stereomicroscope and a polarized microscope, and high quality, inclusion free, nearly spherical, small, and high purity crystals were selected for examination

using single-crystal X-ray diffraction (SCXRD), synchrotron high-resolution powder X-ray diffraction (HRPXRD), and electron-probe micro-analysis (EPMA) techniques.

2.2. Electron-Probe Microanalysis (EPMA)

All chemical analyses (Table 1) were conducted with a JEOL JXA-8200WD-ED electron-probe micro-analyzer (Akishima, Tokyo, Japan). The JEOL operating program on a Solaris platform was used for ZAF (atomic number, Z; absorption, A; fluorescence, F) correction and data reduction. The wavelength-dispersive (WD) analysis was conducted quantitatively using an accelerated voltage of 15 kV, a beam current of 2.0×10^{-8} A, and a beam diameter of 5 μ m. The counting time was 20 s on peak and 10 s on background. Relative analytical errors were 1% for major elements and 5% for minor elements. Various minerals and compounds were used as standards [zircon ($ZrL\alpha$ and $SiK\alpha$), hornblende ($CaK\alpha$, $MgK\alpha$, $FeK\alpha$, $TiK\alpha$, and $AlK\alpha$), hafnium ($HfL\alpha$), YPO_4 ($YL\alpha$ and $PK\alpha$), ThO_2 ($ThM\alpha$), barite ($SK\alpha$), pyromorphite ($PbM\beta$), UO_2 ($UM\alpha$), rhodonite ($MnK\alpha$), NiO ($NiK\alpha$), strontianite ($SrL\alpha$), chromite ($CrK\alpha$), and scapolite ($ClK\alpha$)]. A total of 14 spots were analyzed for each zircon crystal. The quantitative oxide wt.% (both major and trace elements) and the calculated atom per formula unit (*apfu*) for eight samples are given in Table 1. The concentrations of U, Th, and $\Sigma(Hf + TE)$ for 52 zircon crystals are provided in Table 2.

Table 1. Electron-probe microanalysis (EPMA) data for eight zircon samples ⁺.

Wt.%	1:CB	2:CB	3:CB	4:CB	5:BIF	6:HBF	7:PIF	8:JN
ZrO ₂	65.74	65.19	65.09	65.30	63.47	66.35	65.66	65.01
HfO ₂	1.11	1.37	1.59	1.36	1.33	1.11	1.19	1.19
UO ₂	0.02	0.06	0.17	0.08	0.12	0.02	0.03	0.02
ThO ₂	0.01	0.06	0.01	0.08	0.06	0.02	0.03	0.16
PbO	bdl	bdl	0.02	bdl	0.04	0.01	bdl	0.02
CaO	0.02	0.02	0.01	0.02	0.06	0.01	0.02	0.02
Y ₂ O ₃	0.10	0.04	0.04	0.08	0.28	0.03	0.05	bdl
SrO	bdl							
TiO ₂	bdl							
FeO	bdl	0.01	0.01	0.04	0.26	0.01	bdl	0.01
Cr ₂ O ₃	0.01	bdl	bdl	bdl	0.01	bdl	bdl	0.01
MnO	0.01	0.01	0.01	bdl	0.02	0.01	0.01	0.01
MgO	bdl	0.01	0.01	0.01	bdl	0.01	0.01	bdl
NiO	bdl	0.02	0.02	0.02	0.02	bdl	0.01	bdl
SiO ₂	32.67	32.11	32.28	32.75	32.16	31.84	31.34	31.28
P ₂ O ₅	bdl							
SO ₃	0.03	0.04	0.03	0.03	0.03	0.01	0.02	0.01
Al ₂ O ₃	bdl	bdl	bdl	bdl	0.02	bdl	bdl	bdl
Total	99.71	98.93	99.29	99.78	97.89	99.43	98.38	97.75
Atom per formula unit (<i>apfu</i>) based on 4 O atoms								
Zr	0.984	0.987	0.983	0.978	0.969	1.002	1.004	1.000
Hf	0.010	0.012	0.014	0.012	0.012	0.010	0.011	0.011
U	-	-	0.001	0.001	0.001	-	-	-
Th	-	-	-	0.001	0.000	-	-	0.001
Ca	0.001	0.001	-	0.001	0.002	-	0.001	0.001
Y	0.002	0.001	0.001	0.001	0.005	-	0.001	-
Fe	-	-	-	0.001	0.007	-	-	-
Mn	-	-	-	-	0.001	-	-	-
Mg	-	-	-	-	-	0.001	0.001	-
Ni	-	-	-	0.001	0.001	-	-	-
Σ Zr site	0.997	1.003	1.000	0.995	0.998	1.014	1.018	1.014
Si	1.003	0.997	0.999	1.006	1.007	0.986	0.983	0.987
S	0.001	0.001	0.001	0.001	0.001	-	-	-
Σ Si site	1.004	0.998	1.000	1.006	1.008	0.986	0.983	0.987
Total *	2.001	2.001	2.001	2.001	2.006	2.001	2.001	2.001

* Total = sum of all cations; bdl = below detection limit; CB = Cox's Bazar, Bangladesh; BIF = Beverly Inlet Formation; HBF = Hecla Bay Formation; PIF = Parry Island Formation; JN = Jemaa, Nigeria; ⁺ The same sample numbers are used in all the Tables.

Table 2. Concentrations of U, Th, calculated α -radiation dose (α -decay events/mg), and Hf + TE for 52 zircon crystals *.

Sample ID	U (ppm)	Th (ppm)	Radiation Dose	Hf + TE (apfu)	Sample ID	U (ppm)	Th (ppm)	Radiation Dose	Hf + TE (apfu)
1:CB	144	103	4.34×10^{14}	0.014	27	707	186	1.67×10^{15}	0.018
2:CB	494	528	1.36×10^{15}	0.017	28	571	381	1.46×10^{15}	0.023
3:CB	1538	98	3.26×10^{15}	0.019	29	903	458	2.10×10^{15}	0.021
4:CB	669	732	2.82×10^{15}	0.018	30	400	432	1.04×10^{15}	0.017
5:BIF	1058	542	1.48×10^{15}	0.029	31	316	350	8.26×10^{14}	0.015
6:HBF	135	149	2.12×10^{14}	0.013	32	236	466	7.13×10^{14}	0.016
7:PIF	300	254	4.42×10^{14}	0.014	33	1214	286	4.34×10^{15}	0.015
8:JN	208	1370	4.80×10^{15}	0.014	34	2900	387	1.02×10^{16}	0.038
9	498	268	1.45×10^{15}	0.013	35	1690	815	6.36×10^{15}	0.033
10	326	19	8.57×10^{14}	0.019	36	809	560	3.17×10^{15}	0.032
11	340	0	8.83×10^{14}	0.017	37	2779	1775	1.09×10^{16}	0.097
12	164	295	5.97×10^{14}	0.011	38	2280	6861	1.29×10^{16}	0.066
13	848	1097	2.84×10^{15}	0.016	39	4549	3334	1.80×10^{16}	0.148
14	702	239	1.96×10^{15}	0.018	40	1672	1008	6.44×10^{15}	0.069
15	2221	631	6.13×10^{15}	0.028	41	624	379	8.89×10^{14}	0.017
16	1209	311	3.32×10^{15}	0.019	42	90	128	1.49×10^{14}	0.024
17	517	170	1.44×10^{15}	0.014	43	275	445	4.72×10^{14}	0.032
18	510	178	1.42×10^{15}	0.015	44	118	130	1.85×10^{14}	0.016
19	1312	334	3.60×10^{15}	0.021	45	117	0	1.46×10^{14}	0.014
20	127	271	4.86×10^{14}	0.016	46	461	176	6.27×10^{14}	0.019
21	3082	1909	9.10×10^{15}	0.084	47	33	139	8.07×10^{13}	0.014
22	3448	475	9.22×10^{15}	0.093	48	566	243	7.67×10^{14}	0.018
23	869	1898	3.35×10^{15}	0.018	49	0	230	6.53×10^{13}	0.019
24	1935	350	4.49×10^{15}	0.024	50	104	278	2.07×10^{14}	0.017
25	1129	582	2.81×10^{15}	0.019	51	175	46	2.28×10^{14}	0.015
26	1070	63	2.42×10^{15}	0.026	52	72	91	1.15×10^{14}	0.012

* Samples 1 to 7 represent the seven zircon used for the SCXRD work and sample 8 was used for the HRPXRD; samples 9 to 23, 24 to 28, 29 to 32, and 33 to 40 are gray, colorless, pink, and red zircon crystals, respectively, collected from Cox's Bazar, Bangladesh; samples 41 to 44, 45 to 46, and 47 to 52 are BIF, HBF, and PIF zircon crystals collected from the Canadian Arctic Islands.

Thirty six of the 52 zircon crystals are from Cox's Bazar, Bangladesh, 15 are from Canadian Arctic Islands, and one from Jemaa, Nigeria were analyzed. All 52 crystals were analyzed for Hf and trace elements (TE = Ca, U, Th, Pb, Ti, Fe, Sr, Y, Cr, Mg, Mn, Ni, P, S, and Al) using quantitative analyses, as was done for the major elements. The α -radiation doses received by each zircon crystal were calculated for all 52 crystals, but crystals 9 to 52 were not structurally characterized (Table 2).

2.3. Calculation of α -Radiation Dose

To calculate the α -radiation dose using the equation of Holland and Gottfried [15], the age of the zircon sample is needed. The ages for samples 5, 6, and 7 were determined by Anfinson et al. [14] using U-Pb dating that was obtained by LA-ICP-MS. The age of both samples 5 and 6 is 370 Ma, and the age of sample 7 is 365 Ma. The ages of samples 5 (BIF), 6 (HBF), and 7(PIF) were taken from Anfinson et al. [14] and used for the radiation dose calculations in this study.

The ages of zircon samples 1 to 4 and 8 were not previously determined. The concentrations of Pb in these samples are either “zero,” or below detection limit (bdl), except sample 3 (Table 1). Therefore, the concentrations of U, Th, and Pb from the same batch of samples having the same color and similar crystal shapes were selected to calculate their chemical ages using “Montel chemical age equation” [16]. The calculated ages obtained for samples 1 to 4 are: (1) 739, (2) 641, (3) 604, and (4) 948 Ma, and sample 8 is 2384 Ma. The CB beach minerals originated from the nearby exposed Miocene and Pliocene aged Boka Bil and Tipam Formations. The age of zircon grains in the Tipam Formation is between 500 and 1700 Ma, but few grains have Cenozoic and Cretaceous age [17]. Our calculated ages for zircon crystals from Cox’s Bazar fall in the range determined by Najman et al. [17]. The calculated chemical ages of zircon have been used to calculate α -radiation doses. The α -radiation dose (α -decay events/mg) for each zircon sample is calculated from the average U and Th concentrations, assuming that the Pb concentration is zero and using the following Equation (2) from Murakami et al. [18], which is modified from Holland and Gottfried [15]:

$$D = 8N_1[\exp(\lambda^{238} \cdot T)-1] + 7N_2[\exp(\lambda^{235} \cdot T)-1] + 6N_3[\exp(\lambda^{232} \cdot T)-1],$$

where T = is the age of the zircon crystal, D = the dose in α -decay events/mg; N_1 , N_2 , and N_3 = the present numbers of ^{238}U , ^{235}U , and ^{232}Th in atoms/mg; and λ^{235} , λ^{238} , and λ^{232} = the radioactive decay constants (year^{-1}) of ^{235}U , ^{238}U , and ^{232}Th , respectively. The calculated α -radiation doses for the 52 crystals are given in Table 2.

2.4. Single-Crystal X-Ray Diffraction (SCXRD) Data Collection and Structure Refinement for Zircon

A zircon crystal was mounted on the tip of a glass fiber (diameter less than 0.1 mm) using an adhesive. The mounted crystal was placed on a goniometer head and the crystal was centered in the X-ray beam for diffraction measurements. SCXRD data were collected at 295 K with a Nonius Kappa CCD on a diffractometer using Bruker Nonius FR591 Rotating Anode with graphite monochromated Mo-K α radiation ($\lambda = 0.71073 \text{ \AA}$). The generator setting was 50 kV and 36 mA, and the cryostat setting for the diffractometer was set to 295 K (room temperature). The detector-crystal distance was fixed at 35 mm. For unit-cell determination, a total of 10 frames were collected and the scan setting was 1° rotation per frame (total rotation = 10°) and 22 s X-ray exposure time per frame. After obtaining satisfactory unit-cell parameters and mosaicity values (less than 1°), complete data sets were collected using a 2° per frame rotation with X-ray exposure of 42–122 s per frame. The diffraction spots were measured in full, scaled with *Scalepack*, corrected for Lorentz-polarization, and integrated using the Nonius program suite DENZO-SMN (version 2000) [19]. The space group $I4_1/amd$ was obtained based on systematic absent of reflections and structure factor statistics. Full-matrix least-squares refinements were carried out with SHELXL-97 software using neutral atom scattering factors [20]. The WinGX program suite (version 2020.1) was used as the platform for the refinement [21]. The starting structural model was taken from Kolesov et al. [7]. The occupancy factors for Zr, Si, and O sites were assumed to be 1.0. Anisotropic displacement parameters were used for all atoms and the refinement resulted in convergence. Details of the data collection, processing, and refinements are given in Table 3, which also contains the refined extinction coefficients. The refined atom coordinates and displacement parameters are given in Table 4 and selected bond distances and angles are given in Table 5.

Table 3. Single-crystal structure refinement data for seven zircon samples *.

	1:CB	2:CB	3:CB	4:CB	5:BIF	6:HBF	7:PIF
Crystal size (mm)	0.08 × 0.08 ×	0.10 × 0.04 ×	0.08 × 0.08 ×	0.10 × 0.08 ×	0.08 × 0.06 ×	0.10 × 0.08 ×	0.10 × 0.10 ×
Color	Gray	Colorless	Pink	Red	Gray	Gray	Gray
Crystal shape	Spherical	Prismatic	Prismatic	Spherical	Spherical	Spherical	Spherical
Unit-cell parameters (Å)	<i>a</i> 6.6040(9) <i>c</i> 5.9830(6)	6.6030(7) 5.9800(4)	6.6030(5) 5.9780(4)	6.604(2) 5.985(1)	6.6120(7) 5.9970(5)	6.5840(5) 5.9720(5)	6.5790(6) 5.9600(7)
Volume, <i>V</i> (Å ³)	260.94(6)	260.73(4)	260.64(4)	261.0(1)	262.18(4)	258.88(4)	257.97(4)
Density _{calc} (g/cm ³)	4.666	4.670	4.672	4.665	4.644	4.703	4.720
Absorption coefficient (mm ⁻¹)	4.461	4.464	4.466	4.459	4.440	4.496	4.512
2θ range	2°–54.34°	2°–54.70°	2°–54.70°	2°–54.70°	2°–55.16°	2°–54.87°	2°–54.96°
	−8 ≤ <i>h</i> ≤ 8	−8 ≤ <i>h</i> ≤ 8	−8 ≤ <i>h</i> ≤ 8	−8 ≤ <i>h</i> ≤ 8	−8 ≤ <i>h</i> ≤ 8	−8 ≤ <i>h</i> ≤ 8	−8 ≤ <i>h</i> ≤ 8
Index ranges	−8 ≤ <i>k</i> ≤ 8	−8 ≤ <i>k</i> ≤ 8	−8 ≤ <i>k</i> ≤ 8	−8 ≤ <i>k</i> ≤ 8	−8 ≤ <i>k</i> ≤ 8	−8 ≤ <i>k</i> ≤ 8	−5 ≤ <i>k</i> ≤ 6
	−7 ≤ <i>l</i> ≤ 7	−7 ≤ <i>l</i> ≤ 7	−7 ≤ <i>l</i> ≤ 7	−7 ≤ <i>l</i> ≤ 7	−7 ≤ <i>l</i> ≤ 7	−6 ≤ <i>l</i> ≤ 7	−7 ≤ <i>l</i> ≤ 7
Total reflections	442	487	528	487	556	800	255
Unique reflections	88	91	91	91	92	88	85
<i>R</i> _{int}	0.0270	0.0230	0.0224	0.0267	0.0224	0.0252	0.0183
<i>R</i> ₁	0.0125	0.0170	0.0110	0.0133	0.0114	0.0114	0.0121
w <i>R</i> ₂	0.0494	0.0558	0.0483	0.0516	0.0556	0.0542	0.0436
Extinction coefficient	0.026(4)	0.11(1)	0.076(7)	0.005(2)	0.003(2)	0.019(6)	0.039(8)
Largest difference peak/hole (e/Å ³)	0.320 −0.330	0.825 −0.015	0.309 −0.382	0.430 −0.295	0.250 −0.310	0.281 −0.266	0.261 −0.268
Mosaicity (°)	0.616(6)	0.540(5)	0.534(4)	0.85(1)	0.733(5)	0.79(1)	0.843(7)

* Space group = *I*4₁*amd*; formula unit, *Z* = 4 based on ZrSiO₄; F(000) = 344.**Table 4.** Atom coordinates and anisotropic displacement parameters (Å²) obtained with SCXRD for seven zircon samples.

	1:CB	2:CB	* 2a:CB	3:CB	4:CB	5:BIF	6:HBF	7:PIF
Coordinates and <i>U</i> _{ij} for O (<i>x</i> = 0; <i>U</i> ₁₂ = <i>U</i> ₁₃ = 0)								
<i>y</i>	0.0656(2)	0.0657(2)	0.06609(9)	0.0657(2)	0.0659(2)	0.0658(2)	0.0654(2)	0.0659(2)
<i>z</i>	0.1951(3)	0.1953(3)	0.1954(1)	0.1957(2)	0.1948(3)	0.1953(3)	0.1953(3)	0.1950(2)
<i>U</i> _{eq}	0.0094(5)	0.0108(6)	0.0027(2)	0.0097(5)	0.0114(5)	0.0115(5)	0.0124(5)	0.0119(4)
<i>U</i> ₁₁	0.0109(9)	0.0131(9)		0.0128(7)	0.0146(10)	0.0130(9)	0.0142(7)	0.0128(6)
<i>U</i> ₂₂	0.0092(8)	0.0089(8)		0.0095(6)	0.0079(8)	0.0105(8)	0.0116(6)	0.0123(6)
<i>U</i> ₃₃	0.0080(9)	0.0104(10)		0.0067(8)	0.0117(9)	0.0110(9)	0.0116(9)	0.0105(7)
<i>U</i> ₂₃	0.0017(5)	−0.0003(6)		0.0005(3)	−0.0005(5)	−0.0006(4)	−0.0002(5)	0.0002(3)
<i>U</i> _{ij} for Si (<i>x</i> = 0, <i>y</i> = 3/4, <i>z</i> = 5/8; <i>U</i> ₂₃ = <i>U</i> ₁₂ = <i>U</i> ₁₃ = 0)								
<i>U</i> _{eq}	0.0068(5)	0.0064(7)	0.0014(1)	0.0061(6)	0.0081(6)	0.0086(6)	0.0088(6)	0.0083(5)
<i>U</i> ₁₁	0.0070(7)	0.0072(8)		0.0070(7)	0.0083(7)	0.0090(8)	0.0093(8)	0.0090(6)
<i>U</i> ₂₂	0.0070(7)	0.0072(8)		0.0070(7)	0.0083(7)	0.0090(8)	0.0093(8)	0.0090(6)
<i>U</i> ₃₃	0.0065(12)	0.0046(14)		0.0043(12)	0.0076(12)	0.0077(13)	0.0078(13)	0.0070(11)
<i>U</i> _{ij} for Zr (<i>x</i> = 0, <i>y</i> = 3/4, <i>z</i> = 1/8; <i>U</i> ₂₃ = <i>U</i> ₁₂ = <i>U</i> ₁₃ = 0)								
<i>U</i> _{eq}	0.0067(4)	0.0062(5)	0.00023(4)	0.0061(4)	0.0072(4)	0.0081(4)	0.0085(4)	0.0081(4)
<i>U</i> ₁₁	0.0068(4)	0.0066(5)		0.0065(4)	0.0072(4)	0.0080(4)	0.0083(5)	0.0083(4)
<i>U</i> ₂₂	0.0068(4)	0.0066(5)		0.0065(4)	0.0072(4)	0.0080(4)	0.0083(5)	0.0083(4)
<i>U</i> ₃₃	0.0065(6)	0.0056(7)		0.0054(6)	0.0072(5)	0.0083(6)	0.0089(6)	0.0076(5)

* 2a:CB is obtained with HRPXRD.

Table 5. Selected bond distances (Å) and angles (°) obtained with SCXRD for seven zircon samples.

Bond/Angle	# bonds	1:CB	2:CB	* 2a:CB	3:CB	4:CB	5:BIF	6:HBF	7:PIF
Zr-O ^I	4x	2.126(2)	2.126(2)	2.1305(6)	2.127(1)	2.128(2)	2.131(2)	2.119(1)	2.120(1)
Zr-O ^{II}	4x	2.269(2)	2.270(2)	2.2696(6)	2.271(1)	2.267(2)	2.274(2)	2.263(2)	2.259(1)
<Zr-O> [8]		2.198(2)	2.198(2)	2.2001(6)	2.199(2)	2.198(2)	2.203(2)	2.193(2)	2.190(1)
<O-Zr-O> [18]		78.77(5)	78.76(5)	78.761(1)	78.75(4)	78.77(5)	78.76(5)	78.76(5)	78.77(3)
Si-O	4x	1.625(2)	1.624(2)	1.6220(6)	1.622(1)	1.625(2)	1.626(2)	1.622(2)	1.618(1)
<O-Si-O> [6]		109.69(8)	109.69(9)	106.69(1)	109.69(6)	109.70(8)	109.70(9)	109.69(7)	109.70(6)
Zi-Si	2x	2.9920(3)	2.9900(2)	2.9915(1)	2.9890(2)	2.9930(10)	2.9990(3)	2.9860(3)	2.9800(4)
Zr-Zr	2x	3.6250(4)	3.6242(3)	3.6263(1)	3.6240(3)	3.6250(10)	3.6300(3)	3.6147(2)	3.6112(3)

* 2a is obtained with HRPXRD; [] = number of bonds and angles; 4x and 2x = number of equal bonds.

2.5. Synchrotron High-Resolution Powder X-ray Diffraction (HRPXRD)

Fragments of zircon sample 8 from Jemaa, Nigeria and detrital grains of a colorless zircon sample 2a (renaming of sample 2 for the purpose of HRPXRD data) from Cox's Bazar were hand-picked under a stereomicroscope, and crushed into fine powder (<10 µm in diameter) using an agate mortar and pestle for the HRPXRD experiment, which was conducted at beamline 11-BM, Advanced Photon Source, Argonne National Laboratory. The powdered samples were loaded into Kapton capillaries (0.8 mm internal diameter), sealed with glass wool, and rotated during the experiment at a rate of 90 rotations per second. Data were collected to a maximum 2θ of about 50° with a step size of 0.001° and a step time of 0.1 s/step. The HRPXRD data were collected using twelve silicon crystal analyzers that allow for high angular resolution and accuracy, high precision, and accurate diffraction peak positions. A silicon (NIST 640c) and alumina (NIST 676a) standard (ratio of ¹/₃ Si to ²/₃ Al₂O₃ by weight) was used to calibrate the instrument and refine the monochromatic wavelength used in the experiment (Table 6). More technical aspects of the experimental set-up are given elsewhere [22–24]. The experimental techniques used in this study are well established e.g., [25–29].

Table 6. HRPXRD structure refinement data for samples 2a and 8.

Miscellaneous	8:JN	2a:CB
<i>a</i> (Å)	6.6541(1)	6.60700(1)
<i>c</i> (Å)	6.03551(6)	5.98303(1)
<i>V</i> (Å ³)	267.237(7)	261.174(1)
¹ N _{data}	26,246	44,994
² N _{obs}	159	263
³ <i>R</i> (<i>F</i> ²)	0.0395	0.0311
Reduced χ ²	0.8608	2.859
λ (Å)	0.41417(2)	0.459001(2)
2θ range	2°–30°	2°–50°

¹ N_{data} = number of data points; ² N_{obs} = number of observed reflections; ³ *R* (*F*²) = overall R-structure factor based on observed and calculated structure amplitudes = [Σ(*F*_o² - *F*_c²)/Σ(*F*_o²)]^{1/2}.

2.6. Rietveld Structure Refinement

The HRPXRD data for samples 2a and 8 were analyzed with the Rietveld method [30], as implemented in the GSAS program [31], and using the EXPGUI interface [32]. The initial unit-cell parameters and atom coordinates for both samples were taken from Robinson et al. [9]. Scattering curves for neutral atoms were used. The background was modeled using a Chebyshev polynomial (8 terms). The peak profiles were fitted with the pseudo-Voigt function (type-3) in the GSAS program [33]. A full matrix least-squares refinement was carried out by varying the parameters in the following sequence: a scale factor, unit-cell parameters, atom coordinates, and isotropic displacement parameters. The site occupancy factors for Zr and Si were not refined because the chemical analyses showed that these sites are fully occupied (Table 1). In the final stage of the refinement, all parameters were allowed to vary

simultaneously, and the refinement proceeded to convergence. The fitted HRPXRD traces are shown (Figure 2). For sample 8, only the unit-cell parameters are of significance because most of the sample is metamict.

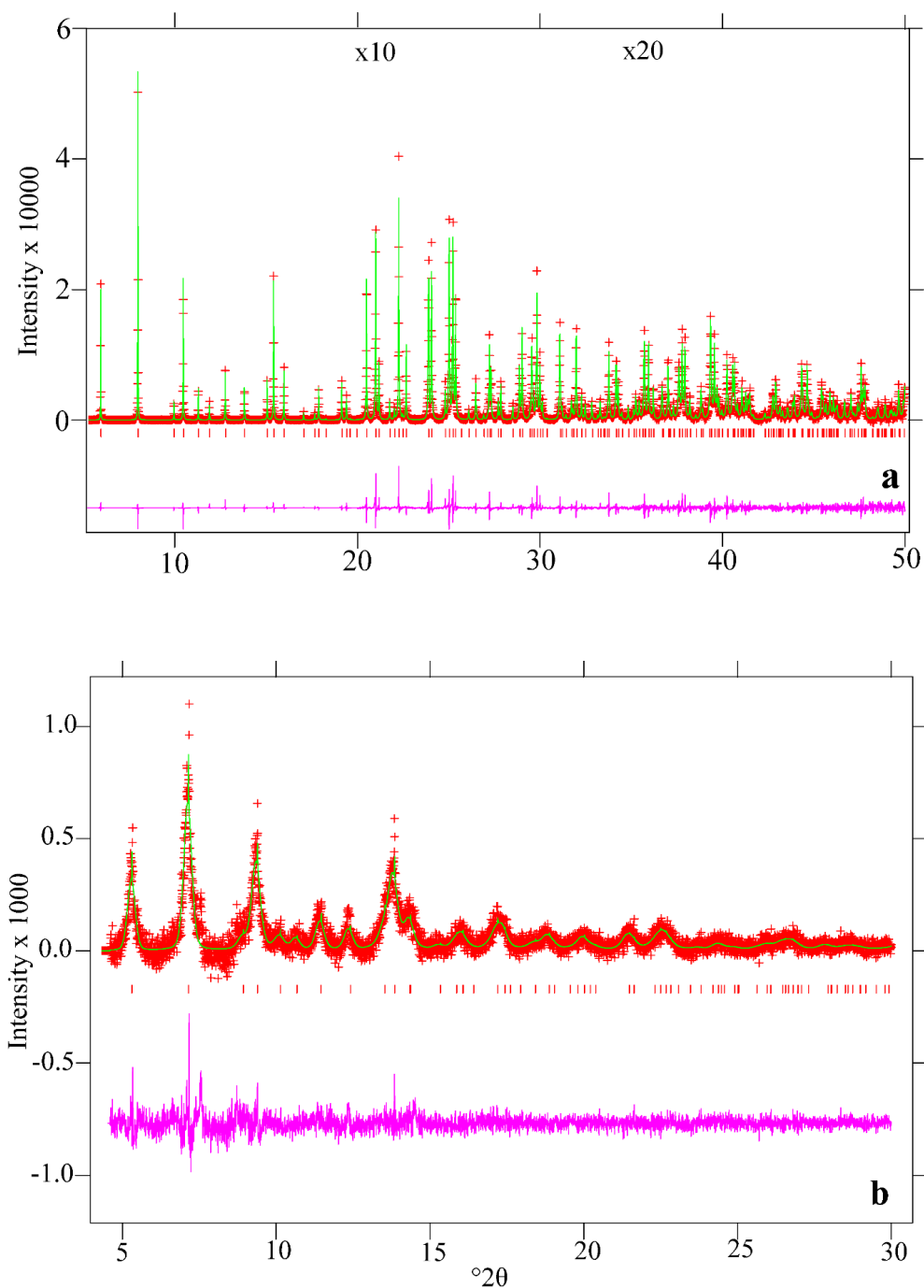


Figure 2. The HRPXRD traces for (a) sample 2a and (b) sample 8 together with the calculated (continuous green line) and observed (red crosses) profiles. The difference curve ($I_{\text{obs}} - I_{\text{calc}}$) is shown at the bottom (pink) at the same scale as the intensity. The short vertical red lines indicate allowed reflection positions. The intensities for the trace and difference curve for sample 2a that are above 20 and 35° 2θ are multiplied by 10 and 20, respectively. The peaks for sample 2a are very sharp and symmetric, and have very high intensity because of high crystallinity. In contrast, the peaks for sample 8 are broad and asymmetric with lower intensity indicating a large amount of amorphous material resulting from α -radiation doses.

The unit-cell parameters, data collection and refinement statistical indicators for samples 2a and 8 are given in Table 6. The atom coordinates and isotropic displacement parameters are given in Table 4. The selected bond distances and angles are tabulated in Table 5.

3. Results

3.1. Chemical Composition of Zircon

Zircon has a stoichiometric composition of 67.2 wt.% ZrO₂ and 32.8 wt.% SiO₂ and may also contain about 20 to 24 trace elements (TE), including Hf and Y as minor elements [34]. The zircon samples from this study have a composition from 63.47 to 66.66 wt.% ZrO₂ and from 31.28 to 32.75 wt.% SiO₂ (Table 1). Zircon may contain Y (0.1 < Y (wt.%) < 1.0), P, and rare earth elements (REE) [34]. The Y concentration in the samples for this study ranges from bdl (sample 8) to 0.28 wt.% (sample 5). The REE-bearing zircon crystals are commonly enriched with P [12]. No P was detected in our samples, so it may be assumed that the REE concentrations are very low (Table 1). The Hf⁴⁺ can replace Zr⁴⁺ cation, as the ionic radius of Hf⁴⁺ (0.83 Å) is almost the same as that of Zr⁴⁺ (0.84 Å) for 8-coordination [35]. Crystalline zircon may contain a mean value of 1.2 wt. % HfO₂, with a range from 0.75 to 1.64 wt.%, whereas metamict zircon may incorporate a mean value of 3.0 wt.% HfO₂, with a range from 1.40 to 6.0 wt.% [36]. All our samples contain HfO₂ from 1.11 (sample 1) to 1.59 wt.% (sample 3), which is close to the HfO₂ concentration for crystalline zircon (Table 1). Typical concentrations of UO₂ and ThO₂ in crystalline zircon fall between 0.06 and 0.40 wt.%, and in metamict zircon fall between 0.20 and 1.5 wt. % [18,36,37].

In this study, all samples contain [0.02 (sample 1) to 0.17 wt.% (sample 3)] UO₂ and is within the range for crystalline zircon. The presence of ThO₂ is less than that of UO₂ and usually range from 0 to 0.20 wt.% in the crystalline zircon and from 0.10 to 1.50 wt.% in the metamict zircon [18,36,37]. ThO₂ concentrations ranges from 0.01 (sample 1) to 0.16 (sample 8) in samples for this study and fall in the range of crystalline zircon as well. Pb²⁺ is not incorporated in zircon when it crystallizes because it is highly incompatible with both Zr⁴⁺ and Si⁴⁺ in terms of its ionic radius (1.29 Å in 8-fold coordination) [37]. However, the radiogenic Pb can develop later because of the decay of ²³⁸U, ²³⁵U, and ²³²Th, but its concentration depends on the time and structural state of zircon, which is key to geochronology. The PbO₂ concentrations in the samples from this study are very low and range from “bdl” to 0.04 wt.% (sample 5). Normally, crystalline zircon contains trace amounts of Ca²⁺, but the metamict zircon incorporates Ca²⁺ in its structure. The presence of Ca²⁺ is the most common indicator of alteration in zircon. The highest amount of Ca²⁺ (0.06 wt.%) is observed in sample 5 (Table 1).

3.2. Variations of Unit-Cell Parameters for Zircon

The *a* and *c* unit-cell parameters increase linearly with increasing unit-cell volume, *V* (Tables 3 and 6, Figure 3). Such linear relations were also observed in other minerals e.g., [38–40]. Unit-cell parameters for undamaged, partially and fully damaged, and synthetic zircon crystals from literature are close to the trend line (Figure 3). The unit-cell parameters for samples 1 to 4 from Cox’s Bazar are similar to each other and they are similar to the values for undamaged zircon studied by Robinson et al. [9] and Siggel and Jansen [41]. The unit-cell parameters for sample 2a is nearly the same as sample 2. Sample 7 has small unit-cell parameters whereas those for sample 8 are the largest because of partial damage by α-radiation (Tables 3 and 6, Figure 3). The unit-cell parameters for zircon generally increase with increasing amount of accumulated α-radiation damage [11,15,18]. Therefore, the small unit-cell parameters for sample 7 may not be related to α-radiation damage. The unit-cell parameters for sample 5 are close to the metamict zircon studied by Mursic et al. [8]. The slopes of the two linear regression lines for the *a* and *c* unit-cell parameters are the same, indicating that the crystal structure changes uniformly in the *a* and *c* directions (Figure 3).

3.3. Relation between Unit-Cell Parameters and Chemical Composition

The variations of the unit-cell volume, V , with the concentrations of Zr and Si are shown in Figure 4. The V increases with decreasing Zr *apfu* and with increasing Si *apfu*. Metamict sample 8 is far away from the two linear regression lines because the V is significantly higher than the other samples. The increase of V for sample 8 is not related to the concentrations of Zr and Si *apfu* (see Figure 5). The large V for sample 8 arises from radiation damage.

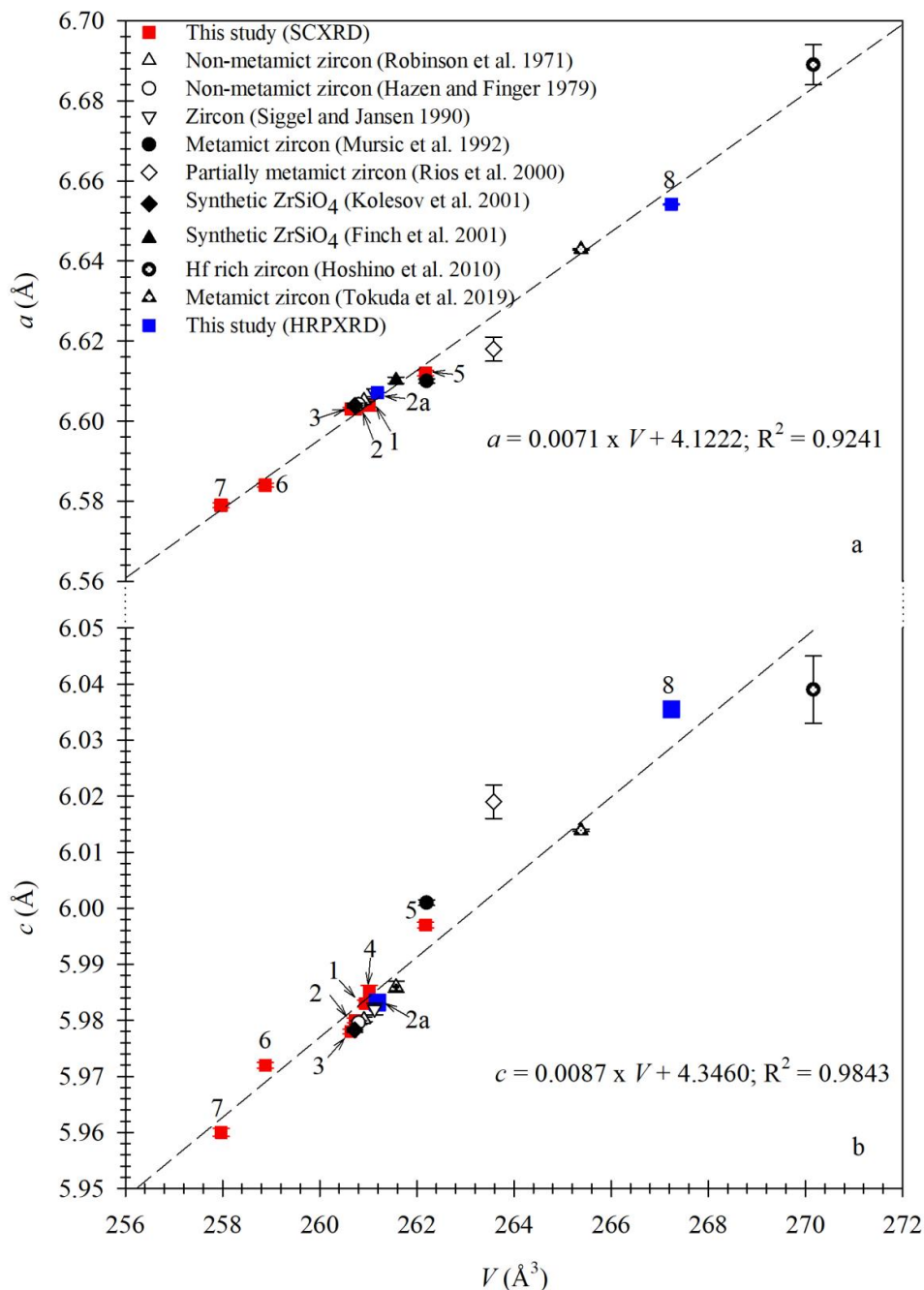


Figure 3. Variations of unit-cell parameters for zircon samples: (a) a with V and (b) c with V . The dashed linear regression lines are based on data from this study and their equations are given as insets. The a and c parameters vary linearly with V . Some data from the literature including those from Tokuda et al. [43] and Hoshino et al. [44] are displayed.

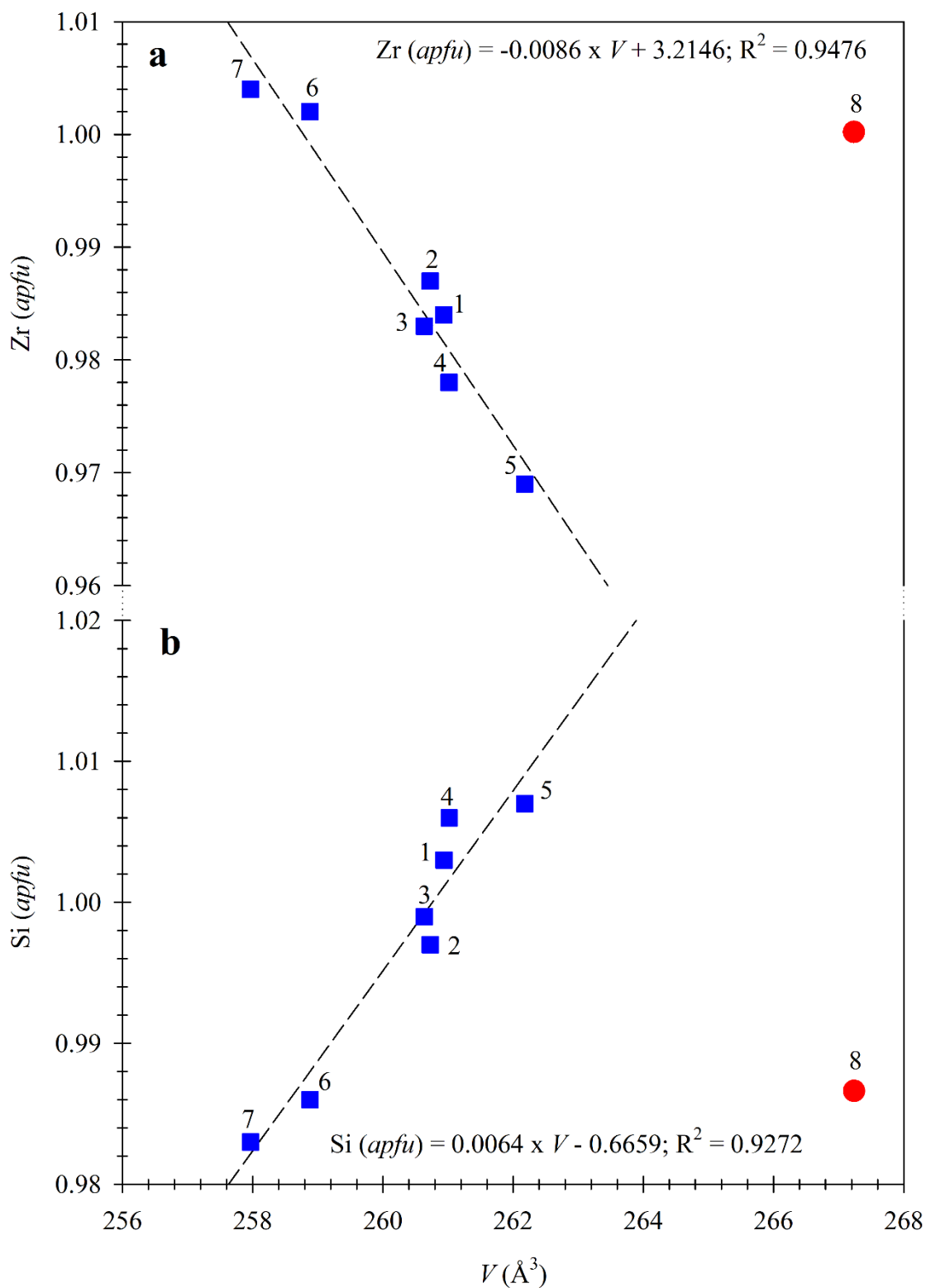


Figure 4. The variations of Zr and Si for the eight zircon samples: (a) Zr with V , and (b) Si with V . The dash lines represent linear fits for samples 1 to 7 and their equations are given as insets. An inverse linear correlation exists between Zr and V in (a). A linear correlation exists between Si and V in (b). The metamict sample 8 is far off the trend lines.

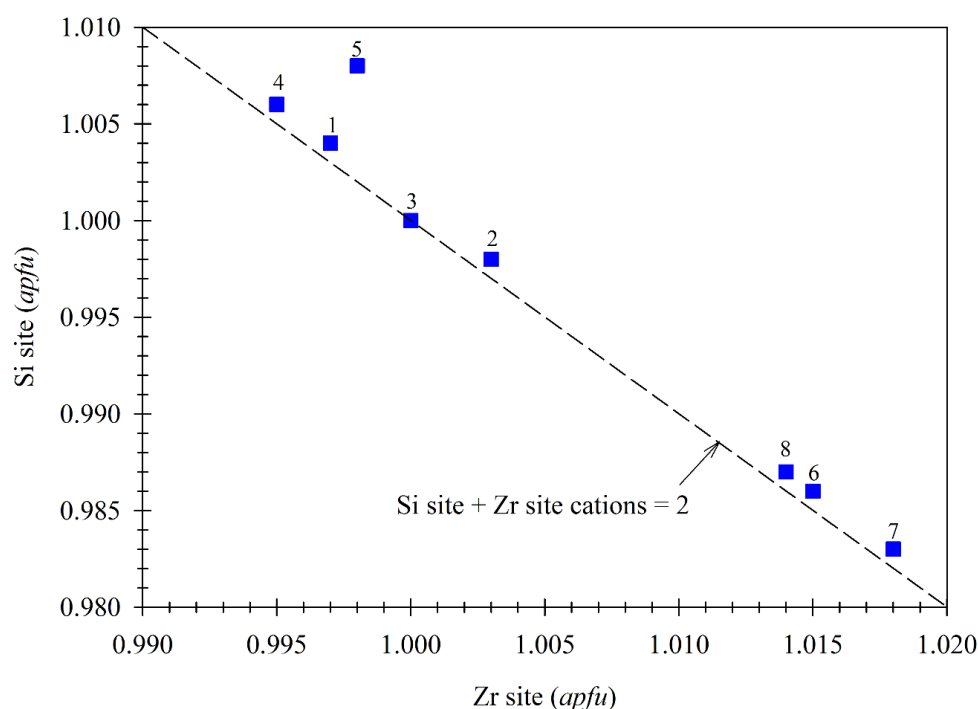


Figure 5. Variation in Zr site cations with Si site cations. Sample 3 has the ideal stoichiometry and the Zr and Si sites are fully occupied. The diagonal dashed line indicates cations sum, $\text{Si} + \text{Zr} = 2$, along which all the zircon samples fall, except sample 5, which does not show ideal stoichiometric composition.

The Hf, U, Th, Ca, Y, Fe, Mn, Ni, and Mg have 8-coordination and close proximity to Zr in terms of their ionic radii, so they substitute for the Zr atom. Only S atom, which has 4-coordination and close in size to Si can substitute for the Si atom. The sum of Zr site cations is plotted against the sum of Si site cations (Table 1, Figure 5). Sample 3 has ideal stoichiometry because the concentration of cations in the Zr and Si sites is 1.0 *apfu* (Table 1). All samples, except sample 5, fall close to a dashed diagonal line representing the sum of Zr and Si site cations = 2 (Figure 5). Samples 6 and 7 show slight non-stoichiometry and display excess cations on the Zr site, which is inversely related to slight deficit in the Si site. Hancher et al. [42] demonstrated that the excess Zr site cations might occupy Si cation site for REE- and P-doped synthetic zircon crystals. The excess Zr site cations in samples 6 and 7 may occupy the Si site or open spaces in the zircon structure. Sample 5 displays the stoichiometric imbalanced relation between Zr and Si site cations. Substitutions for Zr in sample 5 are higher than that for the other samples. Because most of the cations incorporated in sample 5 have ionic radii larger than that of the Zr atom, the *V* increases (Figure 4).

3.4. Relation between Bond Distances and Chemical Composition

The Zr atom is coordinated to eight O atoms and forms ZrO_8 dodecahedra in the zircon structure. Each dodecahedron contains two distinct Zr-O distances (Table 5). The Zr-O^{II} distance is slightly longer than the Zr-O^{I} distance. The Zr-O^{I} distance for sample 6 is ~0.57% smaller and the Zr-O^{II} distance is ~0.09% shorter than that in undamaged zircon [9]. Usually the long Zr-O^{II} distance increases along the [1] direction with increasing amount of radiation damage, whereas there is a small change in the short Zr-O^{I} distance [11]. Therefore, samples 6 and 7 are not affected by radiation damage.

The average $\langle \text{Zr-O} \rangle$ and Si-O distances vary linearly with *V* (Figure 6). Based on the correlation factor, R^2 , the systematic variations of Si-O distances are not as good as the average $\langle \text{Zr-O} \rangle$ distances. The Si-O and $\langle \text{Zr-O} \rangle$ distances are short in sample 7, which is nearly pure zircon. It contains Zr that is close to 1.0 *apfu* and Si that is close to ~0.98 *apfu* (Table 1, Figure 7). There are no other cations in the Si site (e.g., P and S). Thus, the short Si-O distance of 1.618(1) Å for sample 7 is not substitutional

and may represent the pure Si-O distance that is similar to that in quartz where Si-O = 1.608 Å [22]. Sample 5 shows long Si-O and <Zr-O> distances (Figure 6). The reason could be substitutional because the Zr site is not fully occupied (0.969 *apfu*), but the Si site shows full occupancy (1.007 *apfu*). Some cations (e.g., Fe, Y, Ca, etc.) occupy the Zr site in sample 5 that cause the increase in the average <Zr-O> distance (Figure 7).

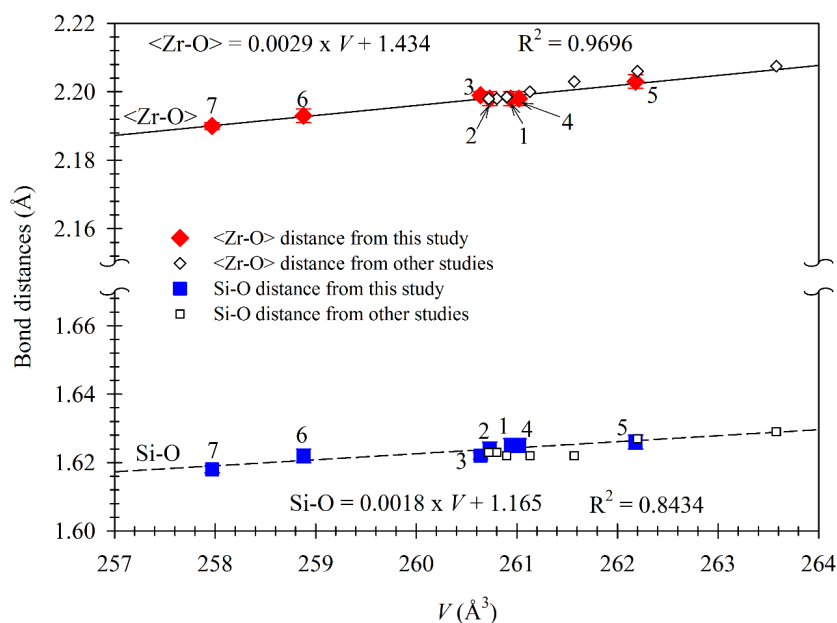


Figure 6. The average <Zr-O> and Si-O distances increase linearly with *V* for the 7 zircon samples. The solid and dashed lines denote linear fits with data from this study and their equations are given as inserts.

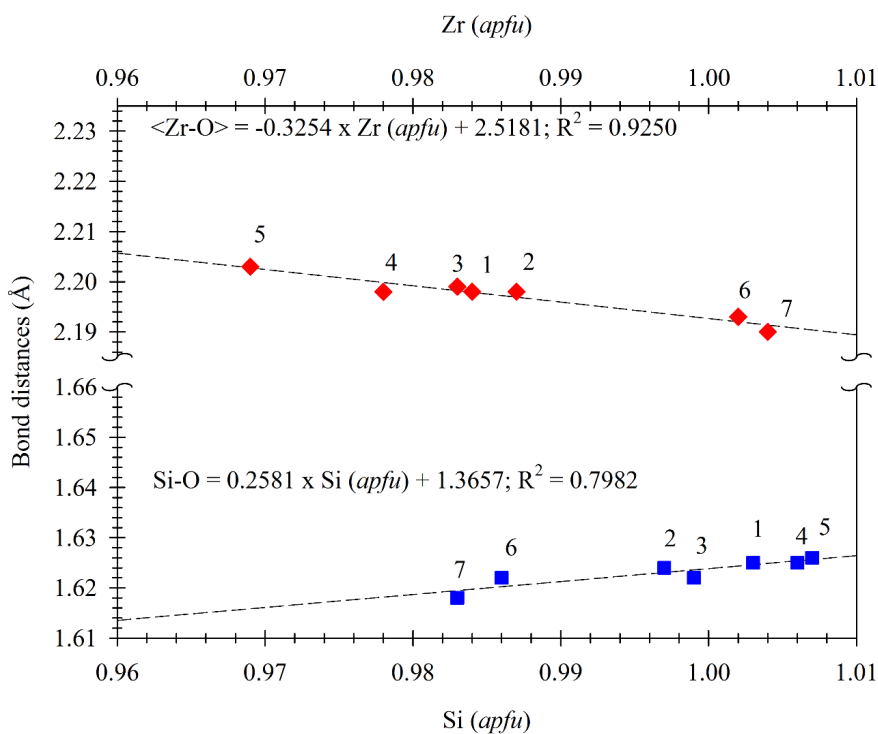


Figure 7. Variations of average <Zr-O> distances with Zr and Si-O distances with Si. The dashed lines denote linear fits and their equations are given as inserts. The Si-O distance increases linearly with increasing Si *apfu*, whereas the <Zr-O> distance decreases linearly with Zr *apfu*.

3.5. Effect of α -Radiation Doses in Zircon

The α -radiation doses are plotted against the $\sum(\text{Hf} + \text{TE})$ *apfu* for 52 zircon crystals and a good polynomial correlation is obtained (Figure 8). The first percolation threshold of the metamictization process occurs at $\sim 3.5 \times 10^{15}$ α -decay events/mg [45]. The isolated amorphous regions resulting from radiation damage are not connected if zircon receives radiation dose below this threshold value. Samples 1 to 7 are relatively unaffected by radiation damage as they received the α -radiation doses that are lower than the threshold value (Figure 8). The maximum amount of radiation dose was received by the metamict sample 8, which is above the threshold value. The α -radiation dose received by sample 8 falls in the range (3.0×10^{15} to 8.0×10^{15} α -decay events/mg), which is the 2nd stage amorphization processes, as explained by Murakami et al. [18]. Because of this high amount of radiation dose, the intensity of the synchrotron HRPXRD peaks decreased and the peaks are broadened compared to crystalline zircon (Figure 2). This indicates that the amorphous zones in the sample increased significantly and give rise to large unit-cell parameters for sample 8. Although the crystal structure contains a large amount of amorphous material, it is still chemically similar to crystalline zircon, as indicated by its stoichiometric composition and minor amount of TE content (Figure 8, Table 1).

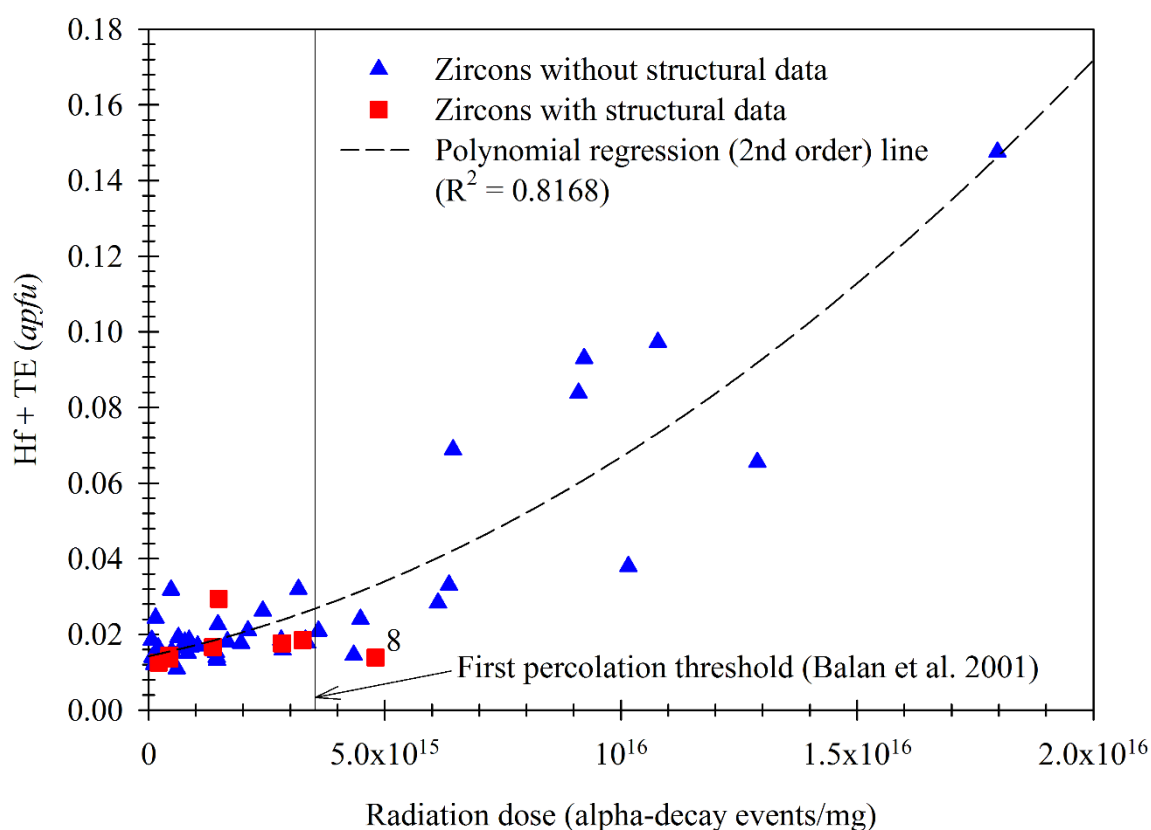


Figure 8. Variations of $\sum(\text{Hf} + \text{TE})$ with radiation dose for 52 zircon crystals (see Table 2). The radiation doses for samples 1 to 7 are below the 1st percolation threshold value (3.5×10^{15} α -decay events/mg). Only the metamict sample 8 received the radiation dose above the 1st percolation threshold value.

3.6. Unit-Cell Volume and Geological Age

The radiation dose for zircon increases with increasing geological age [46]. The control of such age on the unit-cell volume, V , is unknown. However, Figure 9 shows a relation between age and V . Samples 6 and 7 are the youngest zircon samples and have the smallest V . This suggests that they are pure zircon with high crystallinity. Samples 1 to 4 have relatively older ages and have larger V . The metamict sample 8 is oldest and has the largest V . A positive correlation is obtained where V

increases with age (Figure 9). Sample 5 is an outlier and has a high V , although it is relatively young. Some larger atoms (e.g., Fe, Y, Ca, etc.; Table 1) may occupy the Zr site and cause high V for sample 5.

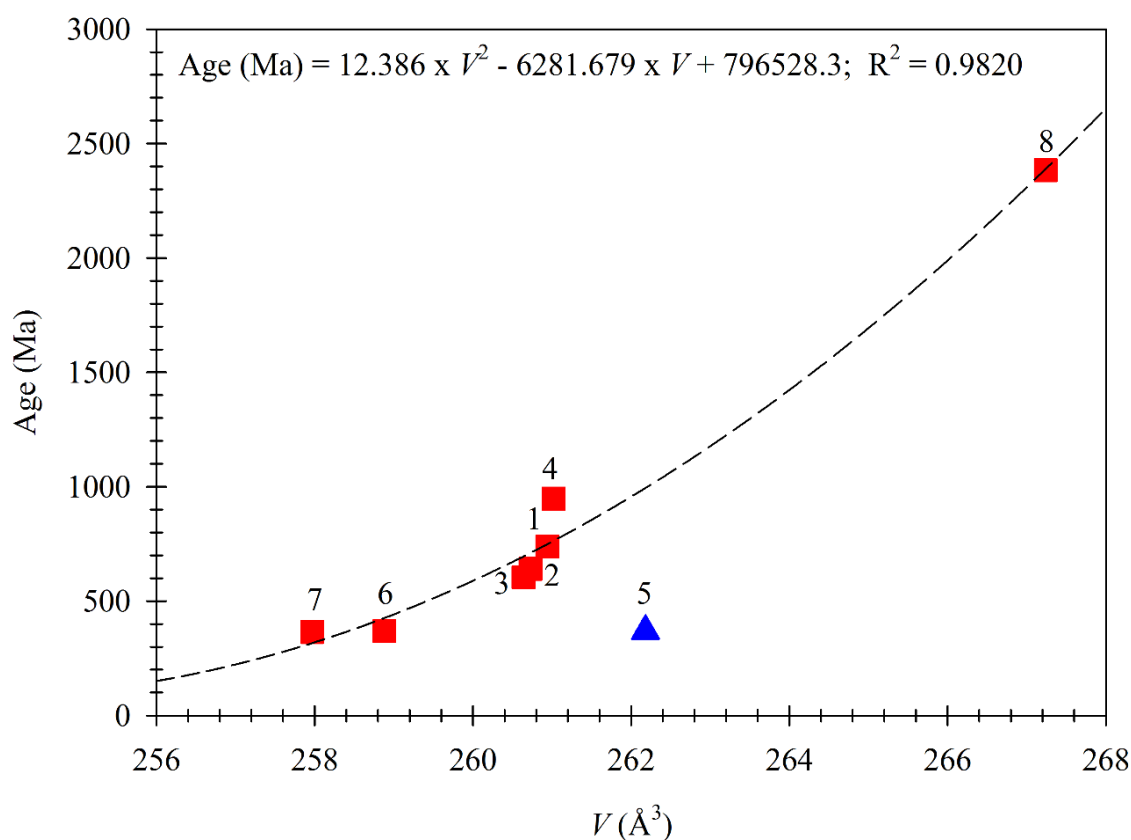


Figure 9. Relation between unit-cell volume, V , and age for zircon crystals. A good 2nd order polynomial fit (dashed line and equation given as insert) exists between V and age for zircon, excluding sample 5 because it has slight non-stoichiometric chemical composition (see Figure 5).

4. Conclusions

This study shows some trends among structural (unit-cell parameters and bond distances), chemical composition (Zr, Si, Hf, and TE), and α -radiation doses. If zircon received low amount of α -radiation doses ($<3.5 \times 10^{15}$ α -decay events/mg), the concentrations of Zr and Si *apfu* control the variations of unit-cell parameters. The smallest unit-cell parameters and bond distances were obtained for sample 7, which received a minor amount of α -radiation doses (4.42×10^{14} α -decay events/mg) over a short time (365 Ma), so the structure is unaffected. Sample 8 received a maximum amount of α -radiation doses (4.80×10^{15} α -decay events/mg) over a long time (2384 Ma) and has the largest unit-cell parameters. Although the V for sample 8 is 3.6% larger than that for sample 7, the stoichiometric proportions of Zr and Si *apfu* are similar to crystalline zircon. A good relation exists between age and V for zircon.

Author Contributions: M.M.Z. carried out the experiments (EPMA, SCXRD) and analyzed the data. S.M.A. carried out the HRPXRD experiment, conceived, and funded the project. Both authors contributed to writing and editing the manuscript. All authors have read and agreed to the published version of the manuscript.

Funding: This research was funded by NSERC Discovery Grant to SMA, grant number 10013896.

Acknowledgments: We thank the four anonymous reviewers for useful comments that helped improve this paper. We thank Masood Parvez for help with the single-crystal X-ray diffraction data collection and Robert Marr for his help with EPMA data collection. The HRPXRD data were collected at the X-ray Operations and Research beamline 11-BM, Advanced Photon Source (APS), Argonne National Laboratory (ANL). Use of the APS was supported by the U.S. Dept. of Energy, Office of Science, Office of Basic Energy Sciences, under Contract No. DE-AC02-06CH11357.

Conflicts of Interest: The authors declare no conflict of interest.

References

1. Vegard, L. VI Results of crystal analysis. *Philos. Mag.* **1916**, *32*, 65–96. [[CrossRef](#)]
2. Hassel, O. Die Kristallstruktur einiger Verbindungen von der Zusammensetzung MRO_4 -I. Zirkon $ZrSiO_4$. *Z. Krist.* **1926**, *63*, 247–254.
3. Krstanovic, L.R. Redetermination of the oxygen parameters in zircon ($ZrSiO_4$). *Acta Crystallogr.* **1958**, *11*, 896. [[CrossRef](#)]
4. Wyckoff, R.W.G.; Hendricks, S.B. Die kristallstruktur von zirkon und die kriterien für spezielle lagen in tetragonalen raumgruppen. *Z. Krist.* **1928**, *66*, 73–102.
5. Finch, R.J.; Hanchar, J.M.; Hoskin, P.W.O.; Burns, P.C. Rare-earth elements in synthetic zircon: Part 2. A single-crystal X-ray study of xenotime substitution. *Am. Mineral.* **2001**, *86*, 681–689.
6. Hazen, R.M.; Finger, L.W. Crystal structure and compressibility of zircon at high pressure. *Am. Mineral.* **1979**, *64*, 196–201.
7. Kolesov, B.A.; Geiger, C.A.; Armbruster, T. The dynamic properties of zircon studied by single-crystal X-ray diffraction and Raman spectroscopy. *Eur. J. Mineral.* **2001**, *13*, 939–948. [[CrossRef](#)]
8. Mursic, Z.; Vogt, T.; Boysen, H.; Frey, F. Single-crystal neutron diffraction study of metamict zircon up to 2000 K. *J. Appl. Crystallogr.* **1992**, *25*, 519–523. [[CrossRef](#)]
9. Robinson, K.; Gibbs, G.V.; Ribbe, P.H. The structure of zircon: A comparison with garnet. *Am. Mineral.* **1971**, *56*, 782–790.
10. Nyman, H.; Hyde, B.G.; Andersson, S. Zircon, anhydrite, scheelite and some related structures containing bisdisphenoids. *Acta Crystallogr.* **1984**, *B40*, 441–447. [[CrossRef](#)]
11. Rios, S.; Salje, E.K.H.; Zhang, M.; Ewing, R.C. Amorphization in zircon: Evidence for direct impact damage. *J. Phys. Condens. Matter* **2000**, *12*, 2401–2412. [[CrossRef](#)]
12. Finch, R.J.; Hanchar, J.M. Structure and chemistry of zircon and zircon-group minerals. In *Zircon*. *Rev. Mineral. Geochem.* **2003**, *53*, 1–25. [[CrossRef](#)]
13. Zaman, M.; Schubert, M.; Antao, S. Elevated radionuclide concentrations in heavy mineral-rich beach sands in the Cox’s Bazar region, Bangladesh and related possible radiological effects. *Isot. Environ. Health Stud.* **2012**, *48*, 512–525. [[CrossRef](#)] [[PubMed](#)]
14. Anfinson, O.A.; Leier, A.L.; Embry, A.F.; Dewing, K. Detrital zircon geochronology and provenance of the Neoproterozoic to Late Devonian Franklinian Basin, Canadian Arctic Islands. *Geol. Soc. Am. Bull.* **2012**, *124*, 415–430. [[CrossRef](#)]
15. Holland, H.D.; Gottfried, D. The effect of nuclear radiation on the structure of zircon. *Acta Crystallogr.* **1955**, *8*, 291–300. [[CrossRef](#)]
16. Montel, J.M.; Foret, S.; Veschambre, M.; Nicollet, N.; Provost, A. Electron microprobe dating of monazite. *Chem. Geol.* **1996**, *131*, 37–53. [[CrossRef](#)]
17. Najman, Y.; Allen, R.; Willett, E.A.F.; Carter, A.; Barfod, D.; Garzanti, E.; Wijbrans, J.; Bickle, M.J.; Vezzoli, G.; Ando, S.; et al. The record of Himalayan erosion preserved in the sedimentary rocks of the Hatia Trough of the Bengal Basin and the Chittagong Hill Tracts, Bangladesh. *Basin Res.* **2012**, *24*, 1–21. [[CrossRef](#)]
18. Murakami, T.; Chakoumakos, B.C.; Ewing, R.C.; Lumpkin, G.R.; Weber, W.J. Alpha-decay event damage in zircon. *Am. Mineral.* **1991**, *76*, 1510–1532.
19. Otwinowski, Z.; Minor, W. Processing of X-ray diffraction data collected in oscillation mode. In *Methods in Enzymology: Macromolecular Crystallography A276*; Carter, C.W., Jr., Sweet, R.M., Eds.; Academic Press: New York, NY, USA, 1997; pp. 307–326.
20. Sheldrick, G.M. A short history of SHELX. *Acta Crystallogr.* **1998**, *64*, 112–122. [[CrossRef](#)]
21. Farrugia, L.J. WinGX suite for small-molecule single-crystal crystallography. *J. Appl. Crystallogr.* **1999**, *32*, 837–838. [[CrossRef](#)]
22. Antao, S.M.; Hassan, I.; Wang, J.; Lee, P.L.; Toby, B.H. State-of-the-art high-resolution powder X-ray diffraction (HRPXRD) illustrated with Rietveld structure refinement of quartz, sodalite, tremolite, and meionite. *Can. Mineral.* **2008**, *46*, 1501–1509. [[CrossRef](#)]

23. Lee, P.L.; Shu, D.; Ramanathan, M.; Preissner, C.; Wang, J.; Beno, M.A.; Von Dreele, R.B.; Ribaud, L.; Kurtz, C.; Antao, S.M.; et al. A twelve-analyzer detector system for high-resolution powder diffraction. *J. Synchrotron Radiat.* **2008**, *15*, 427–432. [[CrossRef](#)] [[PubMed](#)]
24. Wang, J.; Toby, B.H.; Lee, P.L.; Ribaud, L.; Antao, S.M.; Kurtz, C.; Ramanathan, M.; Von Dreele, R.B.; Beno, M.A. A dedicated powder diffraction beamline at the advanced photon source: Commissioning and early operational results. *Rev. Sci. Instrum.* **2008**, *79*, 085105. [[CrossRef](#)] [[PubMed](#)]
25. Antao, S.M.; Hassan, I.; Parise, J.B. Cation ordering in magnesioferrite, $MgFe_2O_4$, to 982 °C using in situ synchrotron X-ray powder diffraction. *Am. Mineral.* **2005**, *90*, 219–228. [[CrossRef](#)]
26. Ehm, L.; Antao, S.M.; Chen, J.H.; Locke, D.R.; Michel, F.M.; Martin, C.D.; Yu, T.; Parise, J.B.; Lee, P.L.; Chupas, P.J.; et al. Studies of local and intermediate range structure in crystalline and amorphous materials at high pressure using high-energy X-rays. *Powder Diffr.* **2007**, *22*, 108–112. [[CrossRef](#)]
27. Ehm, L.; Michel, F.M.; Antao, S.M.; Martin, C.D.; Lee, P.L.; Shastri, S.D.; Chupas, P.J.; Parise, J.B. Structural changes in nanocrystalline mackinawaite (FeS) at high pressure. *J. Appl. Crystallogr.* **2009**, *42*, 15–21. [[CrossRef](#)]
28. Hassan, I.; Antao, S.M.; Parise, J.B. Häüyne: Phase transition and high-temperature structures obtained from synchrotron radiation and Rietveld refinements. *Mineral. Mag.* **2004**, *68*, 499–513. [[CrossRef](#)]
29. Parise, J.B.; Antao, S.M.; Michel, F.M.; Martin, C.D.; Chupas, P.J.; Shastri, S.; Lee, P.L. Quantitative high-pressure pair distribution function analysis. *J. Synchrotron Radiat.* **2005**, *12*, 554–559. [[CrossRef](#)]
30. Rietveld, H.M. A profile refinement method for nuclear and magnetic structures. *J. Appl. Crystallogr.* **1969**, *2*, 65–71. [[CrossRef](#)]
31. Larson, A.C.; Von Dreele, R.B. *General Structure Analysis System (GSAS)*; Los Alamos National Laboratory Report LAUR: Santa Fe, NM, USA, 2000; pp. 86–748.
32. Toby, B.H. Expgui, a graphical user interface for GSAS. *J. Appl. Crystallogr.* **2001**, *34*, 210–213. [[CrossRef](#)]
33. Finger, L.W.; Cox, D.E.; Jephcoat, A.P. A correction for powder diffraction peak asymmetry due to axial divergence. *J. Appl. Crystallogr.* **1994**, *27*, 892–900. [[CrossRef](#)]
34. Hoskin, P.W.O.; Schaltegger, U. The composition of zircon and igneous and metamorphic petrogenesis. In *Zircon. Rev. Mineral. Geochem.* **2003**, *53*, 27–62. [[CrossRef](#)]
35. Shannon, R.D. Revised effective ionic radii and systematic studies of interatomic distances in halides and chalcogenides. *Acta Crystallogr.* **1976**, *32*, 751–767. [[CrossRef](#)]
36. Zhenmin, G.; Jingming, P. Factor affecting metamictization in granites. *Chin. J. Geochem.* **1986**, *5*, 181–188.
37. Harley, S.L.; Kelly, N.M. Zircon, tiny but timely. *Elements* **2007**, *3*, 13–18. [[CrossRef](#)]
38. Antao, S.M. The mystery of birefringent garnet: Is the symmetry lower than cubic? *Powder Diffr.* **2013**, *28*, 281–288. [[CrossRef](#)]
39. Antao, S.M.; Klincker, A.M. Origin of birefringence in andradite from Arizona, Madagascar, and Iran. *Phys. Chem. Miner.* **2013**, *40*, 575–586. [[CrossRef](#)]
40. Antao, S.M. Three cubic phases intergrown in a birefringent andradite-grossular garnet and their implications. *Phys. Chem. Miner.* **2013**, *40*, 705–716. [[CrossRef](#)]
41. Siggel, A.; Jansen, M. Röntgenographische untersuchungen zur bestimmung der einbauposition von seltenen erden (Pr, Tb) und vanadium in zirkonpigmenten. *Z. Anorg. Allg. Chem.* **1990**, *583*, 67–77. [[CrossRef](#)]
42. Hanchar, J.M.; Finch, R.J.; Hoskin, P.W.O.; Watson, E.B.; Cherniak, D.J.; Mariano, A.N. Rare earth elements in synthetic zircon: Part 1. Synthesis, and rare earth element and phosphorus doping. *Am. Mineral.* **2001**, *86*, 667–680. [[CrossRef](#)]
43. Tokuda, M.; Yoshiasa, A.; Kojitani, H.; Hashimoto, S.; Uehara, S.; Mashimo, T.; Tobase, T.; Akaogi, M. The importance of cation–cation repulsion in the zircon–reidite phase transition and radiation-damaged zircon. *Mineral. Mag.* **2019**, *83*, 561–567. [[CrossRef](#)]
44. Hoshino, M.; Kimata, M.; Nishida, N.; Shimizu, M.; Akasaka, T. Crystal chemistry of zircon from granitic rocks, Japan: Genetic implications of HREE, U and Th enrichment. *Neues Jahrb. Mineral. Abh.* **2010**, *187*, 167–188. [[CrossRef](#)]
45. Balan, E.; Neuville, D.R.; Trocellier, P.; Fritsch, E.; Muller, J.P.; Calas, G. Metamictization and chemical durability of detrital zircon. *Am. Mineral.* **2001**, *86*, 1025–1033. [[CrossRef](#)]

46. Lumpkin, G.R.; Ewing, R.C. Alpha-decay damage in minerals of the pyrochlore group. *Phys. Chem. Miner.* **1988**, *16*, 2–20. [[CrossRef](#)]

Publisher’s Note: MDPI stays neutral with regard to jurisdictional claims in published maps and institutional affiliations.



© 2020 by the authors. Licensee MDPI, Basel, Switzerland. This article is an open access article distributed under the terms and conditions of the Creative Commons Attribution (CC BY) license (<http://creativecommons.org/licenses/by/4.0/>).